IVYSPRING INTERNATIONAL PUBLISHER

International Journal of Biological Sciences

2011; 7(6):848-868

Research Paper

Ultrastructural Characterization of Olfactory Sensilla and Immunolocalization of Odorant Binding and Chemosensory Proteins from an Ectoparasitoid *Scleroderma guani* (Hymenoptera: Bethylidae)

Xiangrui Li[1,3], Daguang Lu[2], Xiaoxia Liu[1], Qingwen Zhang[1,✉], Xuguo Zhou[3,✉]

1. Department of Entomology, China Agricultural University, Beijing 100193, China
2. Chinese Academy of Agricultural Science, Beijing,100081, China
3. Department of Entomology, University of Kentucky, Lexington, KY 40546-0091, USA

✉ Corresponding author: Dr. Qingwen Zhang, Department of Entomology, China Agricultural University, Yuanmingyuan West Road, Beijing 100193, China. Phone: 86-10-62733016 Fax: 86-10-62733016 Email: zhangqingwen@263.net or Dr. Xuguo "Joe" Zhou, Department of Entomology, University of Kentucky, S-225 Agricultural Science Center North, Lexington, KY 40546-0091 Phone: 859-257-3125 Fax: 859-323-1120 Email: xuguozhou@uky.edu

Received: 2011.04.14; Accepted: 2011.05.23; Published: 2011.07.17

Abstract

The three-dimensional structures of two odorant binding proteins (OBPs) and one chemosensory protein (CSP) from a polyphagous ectoparasitoid *Scleroderma guani* (Hymenoptera: Bethylidae) were resolved bioinformatically. The results show that both SguaOBP1 and OBP2 are classic OBPs, whereas SguaCSP1 belongs to non-classic CSPs which are considered as the "Plus-C" CSP in this report. The structural differences between the two OBPs and between OBP and CSP are thoroughly described, and the structural and functional significance of the divergent C-terminal regions (e.g., the prolonged C-terminal region in SguaOBP2 and the additional pair of cysteines in SguaCSP1) are discussed. The immunoblot analyses with antisera raised against recombinant SguaOBP1, OBP2, and CSP1, respectively, indicate that two SguaOBPs are specific to antennae, whereas SguaCSP1, which are more abundant than OBPs and detected in both male and female wasps, expresses ubiquitously across different tissues.

We also describe the ultrastructure of the antennal sensilla types in *S. guani* and compare them to 19 species of parasitic Hymenoptera. There are 11 types of sensilla in the flagellum and pedicel segments of antennae in both male and female wasps. Seven of them, including sensilla placodea (SP), long sensilla basiconica (LSB), sensilla coeloconica (SC), two types of double-walled wall pore sensilla (DWPS-I and DWPS-II), and two types of sensilla trichodea (ST-I and ST-II), are multiporous chemosensilla. The ultralsturctures of these sensilla are morphologically characterized. In comparison to monophagous specialists, the highly polyphagous generalist ectoparasitoids such as *S. guani* possess more diverse sensilla types which are likely related to their broad host ranges and complex life styles. Our immunocytochemistry study demonstrated that each of the seven sensilla immunoreacts with at least one antiserum against SguaOBP1, OBP2, and CSP1, respectively. Anti-OBP2 is specifically labeled in DWPS-II, whereas the anti-OBP1 shows a broad spectrum of immunoactivity toward four different sensilla (LSB, SP, ST-I and ST-II). On the other hand, anti-CSP1 is immunoactive toward SP, DWPS-I and SC. Interestingly, a cross co-localization pattern between SguaOBP1 and CSP1 is documented for the first time. Given that the numbers of OBPs and CSPs in many insect species greatly outnumber their antennal sensilla types, it is germane to suggest such phenomenon could be the rule rather than the exception.

Key words: *Scleroderma guani*, OBP, CSP, tertiary structure, sensilla, immunolocalization

Introduction

Scleroderma guani – a biological control agent for longhorned beetles

The ant-like bethylid wasp *Scleroderma guani* (Hymenoptera: Bethylidae) is a generalist ectoparasitoid of wood-boring insects. Indigenous to China, this polyphagous parasitoid can attack more than 50 insect species across 22 families among three orders [1]. *S. guani* has been widely adopted as a biocontrol agent in China to control longhorned beetles, including the Japanese pine sawyer beetle, *Monochamus alternatus* Hope (Coleoptera: Cerambycidae) and the Asian longhorned beetle, *Anoplophora glabripennis* (Motschulsky) (Coleoptera: Cerambycidae).

M. alternatus is the most important insect vector of the pinewood nematode *Bursaphelenchus xylophilus* Steiner et Buhrer in China [2], the causal agent of pine wilt disease. Due to the lack of effective management strategies, pine wilt disease has devastated pine forests in China, Japan, and South Korea. Since 1985, half of the pine trees, *Pinus massoniana*, in China have been wiped out by this disease, and the combined damages and management costs have exceeded 4 billion US dollars annually [3, 4]. Besides intensified quarantine efforts, tree removal, and phytosanitary measures with methyl bromide fumigation [4], biological controls, primarily with parasitic *S. guani,* has shown great promise in combating pine wilt disease though the suppression of Japanese pine sawyer beetle [4].

It is worth noting that *S. guani* is fairly effective in controlling the Asian longhorned beetle as well. *Anoplophora glabripennis*, native to China, is believed to be introduced to the U.S. through wood pallets used in cargo shipments in the late 1980s. Since the initial discovery of *A. glabripennis* in New York in 1996, it has been found in other parts of the US, Canada, and recently in Austria and France. One of the most destructive woodborers, *A. glabripennis* is a serious invasive threat to North American and European forests. It attacks and kills many hardwood trees, and it can significantly disrupt the forest ecosystem if established. *Scleroderma guani*, a natural enemy for *A. glabripennis* in China, is currently under investigation as a potential biological control agent to manage Asian longhorned beetles in the US [5, 6].

Antennal sensilla

Antennae of insects function to sense odor, sound, humidity, and tactile information. Although it varies greatly among insects, antennae have three basic segments including scape, pedicel and sub-segmented flagellum. Every segment is covered with numerous antennal sensilla, which typically occur in the form of hairs, pegs or plates [7]. Antennal sensilla can be subcategorized into chemosensilla (e.g., olfactory and gustatory receptors) and mechanosensilla (e.g., touch receptors) by their different sensory roles [8]. Alternatively, based on their structural distinctions, sensilla can be classified into multiporous, uniporous, and aporous sensilla [8]. In general, sensilla with pores serve as chemosensilla, whereas aporous sensilla are predominantly associated with touch-, thermo-, and hygroreception [9]. The abundance and distribution of pores vary greatly. For example, they can be distributed ubiquitously throughout the entire sensilla wall or there can be a single pore found at the tip of a sensillium [8].

Parasitic hymenopterans are typically equipped with specialized sensory organs such as antennal sensilla to facilitate their biological functions. To better understand the chemical communication of these potential biological control agents, the ultrastructure of antennal sensilla has been studied extensively in various species of Hymenoptera parasitoids using electron microscopy techniques [10-23].

Odorant binding proteins and chemosensory proteins

Within the sensilla, the dendrites of olfactory neurons are surrounded by highly concentrated olfactory proteins in the sensilla lymph. These small amphipathic proteins serve as carriers to transport the hydrophobic molecules across the aqueous sensillar lymph to reach the olfactory receptors. Odorant binding proteins (OBPs) and chemosensory proteins (CSPs) are two of the best known olfactory proteins in insects [24, 25].

The OBPs, subdivided into pheromone binding proteins (PBPs), general odorant binding proteins (GOBPs) and antennal specific proteins (ASPs) or antennal-binding protein x (ABPx), have been extensively studied in various insect orders, e.g., Coleoptera [26], Dictyoptera [27], Diptera [28], Hemiptera [29], Hymenoptera [30], Isoptera [31], Lepidoptera [32], and Orthoptera [33]. The CSPs, previously referred to as OS-D-like proteins [34] and sensory appendage proteins [35], have been identified in Phasmatodea, Orthoptera, Lepidoptera, Hymenoptera, Diptera, Hemiptera, Coleoptera, Dictyoptera, Siphonaptera, and Phthiraptera [33, 36-40].

Although CSPs share no sequence similarity with OBPs, these two groups of carrier proteins are characterized structurally by a hydrophilic surface and a hydrophobic core, respectively, to make them soluble in the sensillar lymph and to enable them to bind and carry olfactory ligands. Both OBPs and CSPs have the α-helical structure which is a common fea-

ture in many other lipid binding/carrying proteins [41-43]. However, the spatial configurations of α-helices differ greatly between OBPs and CSPs, and such differences are partially explained by the cysteine residues in both peptides. Extensive bioinformatics analyses with existing genomics information revealed that the most reliable "signature motif" among all the OBPs and CSPs is their highly conserved cysteine motif (C-pattern) with specific spacing between residues [44, 45]. Typically, OBPs have six cysteines which form three interlocked disulfide bridges to tightly link the antiparallel helices, whereas, the helical structure of CSPs are relatively flexible because α-helices are connected by a pair of small loops. These loops are generated by the disulfide bridges between two sets of adjacent cysteines.

Despite their pronounced structural differences, OBPs and CSPs share a similar function. The structural differences, especially in the ligand binding pockets, among OBPs and CSPs may dictate the repertoire of small olfactory ligands each protein can bind. Nevertheless, the primary functions of OBPs and CSPs are to enhance the solubility of hydrophobic odorant molecules, to prevent their degradation, and to deliver them throughout the aqueous sensillar lymph to reach specific receptor proteins embedded in the dendritic membrane [46]. The highly evolved and complex structures of OBPs, however, enable them to have additional functions. They could serve as a i) scavenger for removing the excess pheromones to maintain receptor activity [47]; ii) filter to reduce the concentration of odorants to avoid the long-term receptor desensitization [47]; and iii) activator for specific olfactory receptor [48].

Parasitoid-host interactions have been a text book model for the study of chemical communication among insects [49]. As a biological control agent for an invasive Asian longhorned beetle currently ravaging North America, there is added incentive to introduce this polyphagous parasitoid into the New World. Understanding the chemoreception is essential for host preference and localization behaviors in *S. guani* [50]. The olfactory sensilla and olfactory proteins including odorant binding and chemosensory proteins are an integral part of this chemosensory environment, and warrant further investigation. Previously, two OBPs and one CSP were identified from *S. guani* antennae [51]. As a continuation of previous cloning efforts, we characterized the three-dimensional structures of SguaOBP1, OBP2, and CSP1 using an online protein structure homology-modeling server, SWISS-MODEL. We then resolved the ultrastructure of the olfactory sensilla on the flagellum and pedicel segments of *S. guani* antennae using electron microscopy technology. Finally, we carried out immunocytochemistry to localize olfactory proteins in specific olfactory sensilla using antisera developed for recombinant SguaOBP1, OBP2, and CSP1, respectively.

Materials and Methods

Bethylid wasp

Scleroderma guani colonies were maintained at 28°C and 70% RH under complete darkness in a 10ml-glass container. The parasitoids were provisioned with larvae of yellow mealworm beetle, *Tenebrio molitor* L. (Coleoptera: Tenebrionidae), as hosts. The adult wasps were stored at 10°C after emergence prior to dissection.

In silica structural analysis

The signal peptides of *S. guani* OBPs and CSP were predicted by SignalP (http://www.cbs.dtu.dk/services/SignalP/). Amino acid sequences of CSPs from *S. guani* (ABE68832) and *Nasonia vitripennis* (XP_001601633) were aligned using ClustalW (http://www.ebi.ac.uk/Tools/msa/clustalw2/). The three-dimensional structures of OBPs and CSP were simulated by an online protein structure homology-modeling server, SWISS-MODEL (http://swissmodel.expasy.org/). First, the target amino acid sequence from *S. guani* was blasted against the RCSB Protein Data Bank (PDB) to identify an optimal template. Then, the target sequence was subjected to the SwissModel automated mode to construct the 3-D structure using the optimal template obtained from the first step. Finally, PyMOL-v1.3r1 (Delano Scientific LLC.; http://pymol.org/) was used for molecular visualization and labeling of important structural features such as α-helices and disulfide bridges.

Recombinant protein expression, optimization, and purification

A recombinant expression plasmid was constructed by ligating the cDNAs encoding ORFs without signal peptides of *S. guani OBP1*, *OBP2* and *CSP,* respectively, into a bacterial expression vector pET-28a (+) (Novagen, Madison, WI) following their protocols. These cDNAs were amplified by PCR using primer sets specified in **Supplementary Material: Table S1**. The sense primers (OBP1-S, OBP2-S and CSP1-S) were designed to include an *Nde*I restriction site upstream of the start codon. The anti-sense primers included either BamHI restriction site (OBP1-ASf) or *Eco*RI restriction site (OBP2-ASf and CSP1-ASf) downstream of the stop codon.

The resulting plasmidic DNAs were used to transform *E. coli* BL21 (DE3) cells. Positive clones,

confirmed by PCR amplification and direct sequencing to contain OBP1, OBP2 and CSP1 fragments, were grown at 37°C overnight, respectively, in 10ml Luria-Bertani/Miller broth medium containing 100 mg/l Kanamycin, followed by a 1:100 (v/v) dilution in fresh medium until the OD_{600} value reached 0.4-0.6. To optimize the recombinant expression and to maximize the production of soluble protein, a series of induction conditions were investigated, including isopropyl β-D-thiogalactopyrano side (IPTG) concentration (0, 0.2, 0.4, 0.6, 0.8 and 1 mM), incubation temperature (25 and 37°C), and incubation time (0, 1, 3, 7, 10, and 18h). For the production of recombinant proteins, confirmed positive clones were grown and induced in a 1000 ml LB medium with constant shaking (180rpm) under the optimal condition. Thereafter, the cells were harvested by centrifugation at 4,000 x g for 20 min, resuspended in the lysis buffer (50 mM NaH_2PO_4, 300 mM NaCl, pH 8.0) at 80 ml per gram wet weight. The cells were lysed by sonication in an ice bath using a sonicator equipped with a microtip (6 cycles of 10s bursts at 200-300 W followed by 10s cooling period in between each burst until the solution became clear). The lysates were centrifuged at 12,000 × g for 20 min at 4°C, and the soluble and the insoluble fractions were analyzed by SDS-PAGE (polyacrylamide gel electrophoresis). The resulting supernatant was first passed through a sterile filter (0.2μm) to remove free particles, and then the cleared lysate was placed into the Ni-NTA Superflow Syringe (Qiagen) to purify the His-tagged proteins following the manufacturer's protocols.

S. guani antisera production

Polyclonal antisera against recombinant *S. guani* OBP1, OBP2 and CSP1, respectively, were obtained by consecutive 4-week injection (500mg first two weeks, and 300mg for the final two weeks) of purified recombinant proteins into respective rabbits. Each recombinant protein was emulsified with an equal volume of Freund's complete adjuvant (Sigma, St. Louis, MO) for the first injection and incomplete adjuvant (Sigma, St. Louis, MO) for the remaining injections. Animals were bled 10 days after the last injection and the serum supernatant was obtained at 4 °C, 12,000 rpm for 15 min.

Immunoblot analysis

Adult wasps were anesthetized on ice. Antennae of female were dissected under the microscope using forceps and immediately transferred into a 1.5ml Eppendorf microcentrifuge tube that was immersed in liquid nitrogen. Antennae were stored at -80°C. For protein extraction, adult wasps were homogenized in an ice-cold glass homogenizer with 20mM Tris-HCl, pH 7.4, and then centrifuged twice at 12,500 x *g* for 10 min at 4°C. The supernatants were dried using a speed vacuum (EZ550Q, Ultralow Freezer System, FTS Systems Inc., Stone Ridge, NY, USA). Protein concentration was quantified by the Bradford assay. A gradient of protein concentrations (7.5, 15, 30, 60, 120μg) was examined to optimize the immunoblot analysis. Total proteins from male and female wasps, and from different tissues of female wasps, including abdomen, thorax, head, leg, and antennae, were extracted and standardized to 7.5μg per sample. After electrophoretic separation, protein bands were transferred from a 15% SDS-PAGE to a nitrocellulose membrane (0.2μm, Millipore, USA) according to [52]. After treated with 0.2% non-fat dry milk and 0.05% Tween-20 in PBS overnight, the nitrocellulose membrane was then incubated with the primary antiserum obtained previously at a dilution ranging from 1: 1000 to 1: 6000. Goat anti-rabbit IgG- horseradish peroxidase conjugate (diluted by 1: 1000; Fermentas, MD) was used as the secondary antibody. Immunoreactions were visualized by adding 5-bromo-4-chloro-3-indolyl-phosphate and 4-chloro-1-naphthol (Promega, WI).

Immunolocalization

Antennae were chemically fixed in a mixture of paraformaldehyde (4%) and glutaraldehyde (2%) in 0.1 M PBS (pH 7.4), dehydrated in an ethanol series and embedded in LR White resin with polymerization at 60°C. Ultrathin sections (60–80 nm) were cut with a glass knife on a RMC MT-XL or with a diamond knife on a Reichert Ultracut ultramicrotome (Reichert Company, Vienna, Austria). For immunocytochemistry, the grids were subsequently floated on 30 ml droplets of the following solutions: PBS (containing 50 mM glycine), PBGT (PBS containing 0.2% gelatine, 1% bovine serum albumin and 0.02% Tween-20), primary antiserum diluted with PBGT, six changes of PBGT for washing, secondary antibody diluted with PBGT, twice each on PBGT, PBS glycine, PBS and water. Optional silver intensification increased the size of the gold granules from 10 to about 40 nm, and 2% uranyl acetate increased the tissue contrast for observation in the transmission electron microscope (HITACHI H-7500 or Zeiss EM 10A). The primary antisera were examined at a dilution ranging from 1:500-1: 6000 for OBPs and 1: 3000-1: 10000 for CSP, and incubated at 4°C overnight. As a negative control, the serum supernatant from an uninjected healthy rabbit at the same dilution rate was used as the primary antiserum. The secondary antibody, anti-rabbit IgG which coupled to 10-nm colloidal gold (AuroProbe EM, GAR

G10; Amersham, Biosciences, Little Chalfont, Buckinghamshire, UK), was diluted 1: 20 and then incubated at room temperature for 60-90 min. Immunocytochemical labeling was carried out on sections of ten adult wasps from each sex.

Scanning electron microscopy (SEM)

For scanning electron microscopy (SEM), the antennae of adult males and females were cut into several parts and fixed in 70% ethanol for 2 h, and then cleaned in an ultrasonic bath (250 W) for 1 min in the same solution. After treatment with 100% ethanol for 30 min, the samples were air dried. The prepared specimens were mounted on aluminum stubs and coated with gold/palladium (40: 60) in a Polaron E 5400 high-resolution sputter. During sputtering, the chamber pressure was maintained at 5 Pa. The obtained gold layer was thinner than 10 nm, and could not affect the morphology of the specimens. The SEM images were obtained by a HITACHI S570 (Hitachi Ltd., Tokyo, Japan) or FEI Quanta 200 SEM (FEI Company, the Netherlands).

Transmission electron microscopy (TEM)

For TEM, male and female antennae were fixed with a mixture of 5% sucrose and 2.5% glutaraldehyde in 0.1 M phosphate buffer solution (PBS, pH 7.4) for 6 hr at room temperature. Antennae were then rinsed ten times with a washing solution containing 0.1M PBS (pH 7.4) and 6.8% sucrose for 20min each, followed by dehydration in an ethanol series and 100% acetone. Embedding was done via propylene oxide in Epon 812. Ultrathin sections were cut with a glass knife on a LKB V Ultramicrotome and mounted on Formvar-coated grids. The specimens were observed in a HITACHI H-7500 (Hitachi Ltd., Tokyo, Japan).

Statistical analysis

The antennae of *S. guani* are composed of scape, pedicel, and 11-segmented flagellum. Antennae from male and female wasps were documented by scanning electron micrographs, and the length of each segment and the entire antennae were measured. Measurements obtained from photomicrographs of at least 10 individuals were used to calculate means.

Data were analyzed the Student t-test using the Statistical Analysis System (SAS) Version 8.01 (SAS Institute, Cary, NC) to examine differences in length between male and female antennae.

Results

Structural analysis

Based on *in silico* simulation (templates used in SWISS-MODEL are 3d76A, 3bjhA, and 2jntA for SguaOBP1, OBP2, and CSP1, respectively), SguaOBP1 and 2 are classic OBPs with a "signature" six-cysteine C-pattern. SguaCSP1, however, belongs to a rare, non-classic CSP group with two additional conserved cysteines, which we refer to as the "Plus-C" CSPs according to the naming system for OBPs [44, 45, 53]. The amino acid distances between cysteine pairs are generally in congruence with the C-patterns for Hymenoptera. Specifically, SguaOBP1 and 2 follow exactly the C1-X23-35-C2-X3-C3-X27-45-C4-X7-14-C5-X8-C6 motif, whereas SguaCSP1 is consistent with the C1-X6-8-C2-X18-19-C3-X2-C4 motif up to the fourth cysteine residue [44]. The three and eight amino acids between the C2-3 (C61-C65 in OBP1 and C57-C61 in OBP2) and C5-6 (C113-C122 in OBP1 and C110-C119 in OBP2), respectively, in SguaOBPs, and the two residues between the C3-4 (C77-C80) in SguaCSP1 are strikingly conserved throughout different insect taxa **(Fig. 1A&B)**.

The overall 3-D structures of SguaOBPs are roughly a globular shape with four antiparallel α-helices (α1, 4, 5, and 6) enclosing the hydrophobic ligand binding pocket. Helix α3 is stabilized by two disulfide bridges (C34-C65 and C61-C113 in OBP1 and C34-C61 and C57-C109 in OBP2) that anchor it to helices α1 and α6 and serve as the base for the binding pocket. The third disulfide bridge (DBIII, C104-C122 in OBP1 and C99-C119 in OBP2) tightly locks helices α5 and α6 together **(Fig. 1C&D)**.

On the other hand, the helical structure of SguaCSP1 also results in a globular shape **(Fig. 2A)**. However, the spatial configuration of participating helices is different from that of SguaOBPs. Specifically, helices α1-α2 and α4-α5 form two V-shaped structures with helix a3, perpendicular to the two planes, serving as the base for the binding pocket **(Fig. 2B)**. Two small loops generated by disulfide bridges I and II (C49-C58 and C77-C80, respectively) connect the helical structures of SguaCSP1. The structural significance of an additional pair of cysteine residues (C96 and C129) is extremely intriguing because CSPs are considered to be highly conserved in their C-patterns in comparison to the evolutionarily divergent OBPs [44, 45]. The locations of C5 and C6 on the 3-D structure of SguaCSP1 are not specified due to the lack of appropriate protein template representing this newly discovered Plus-C CSP in the SWISS-MODEL **(Fig. 2B)**.

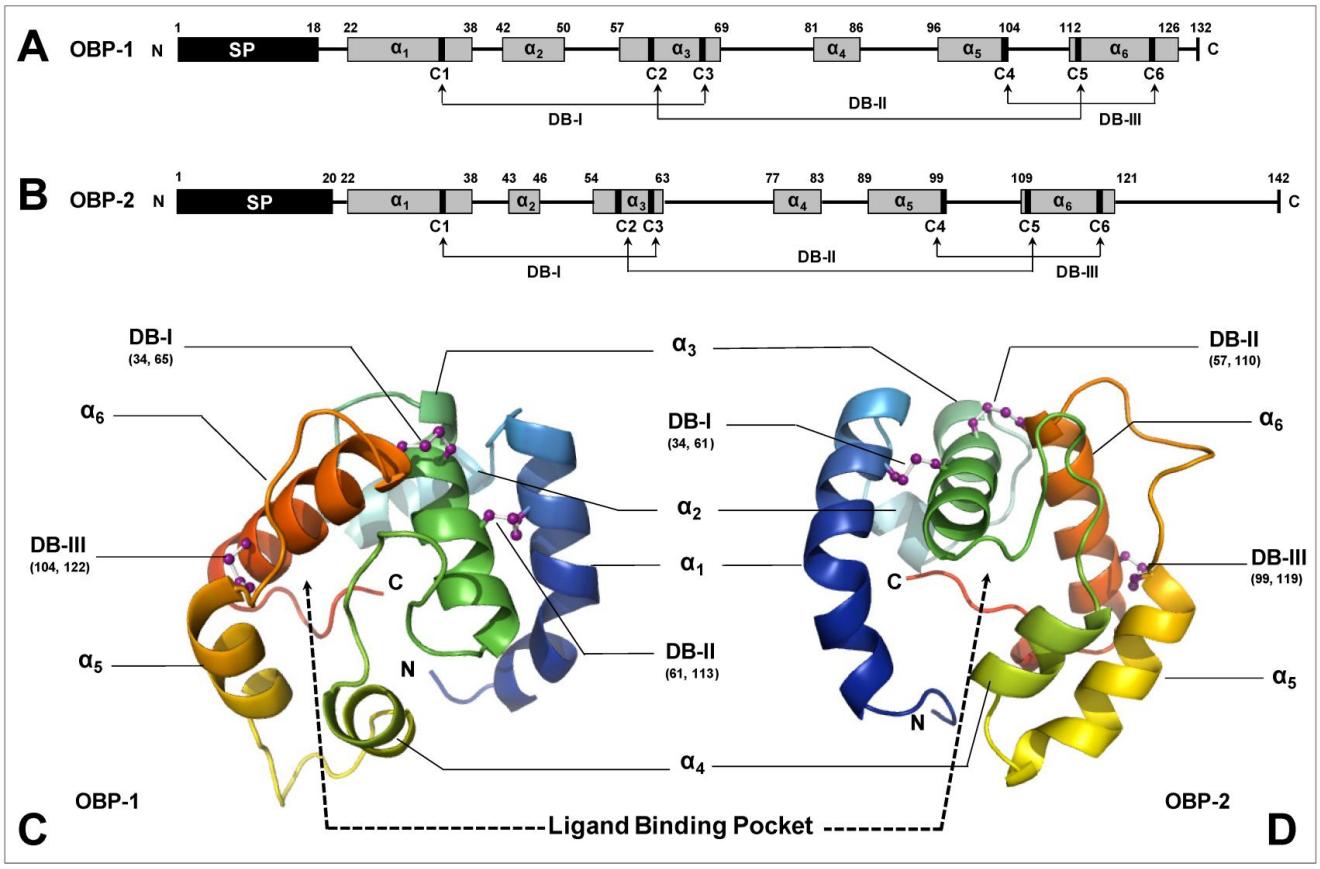

Figure 1. Schematic drawing of three-dimensional structures of *S. guani* OBPs. Primary structures of SguaOBP1 and SguaOBP2 are depicted in A and B, respectively, whereas their three-dimensional tertiary structures are simulated in C and D, respectively. Predicted signal peptides (SP) and α-helices are illustrated in black and grey boxes, respectively. Six highly conserved cysteine residues (C1-6) covalently form three interlocked (C1-3, C2-5, and C4-6) disulfide bridges (DBs) to stabilize the three-dimensional structure of OBP. The α-helices, namely α1-6, are color coded in the tertiary structure (C and D), and their anti-parallel spatial arrangements are simulated based on the selected protein template from SWISS-MODEL. N- and C-terminus, disulfide bridges, and the putative ligand binding pocket are highlighted in the simulated S. guani OBP tertiary structure.

Nevertheless, the spatial proximity between the helix α4-bound C5 and the C-terminus-bound C6 suggests the potential formation of the third disulfide bridge (DBIII, C96-C129) in SguaCSP1. Based on the Blast search result, the only other "Plus-C" CSP deposited in the GenBank is the one from *Nasonia vitripennis* **(Fig. 2C)**. Both *S. guani* and *N. vitripennis* are ectoparastic wasps with a broad range of host species, and not surprisingly, CSPs from these two parasitoids share the highest sequence identity at the peptide level (42%).

Recombinant protein expression and immunoblot analysis

Five concentrations of IPTG, two temperature settings, and five incubation times were examined to maximize the cytosolic induction of recombinant SguaOBP1, OBP2 and CSP1, respectively. The optimal condition was determined to be 0.4mM IPTG, at 25°C for 7 hours using a truncated ORF construct without the signal peptide because 1) the induction of recombinant *S. guani* proteins by IPTG showed no significant improvement beyond 0.4mM concentration, 2) the yield of soluble recombinant protein was greatly reduced at 37°C, although the production of *S. guani* recombinant protein was increased at a higher incubation temperature (mainly formed inclusion body), 3) the production of recombinant *S. guani* proteins showed no significant improvement beyond 7-hour incubation time, and 4) there was no recombinant production with the complete ORF construct, i.e., recombinant *S. guani* protein can only be expressed as a mature protein in *E. coli* (XL, unpubl. data). Under the optimal conditions **(Fig. 3A)**, 100 ml of bacteria cul-

ture produced 0.3038±0.0242 (n=4), 0.7658±0.0539 (n=4), and 0.4682±0.0303 mg of soluble OBP1, OBP2, and CSP1 after a single step purification procedure (Ni-NTA Superflow Syringe).

The polyclonal antisera raised against the recombinant proteins clearly recognized the target *S. guani* OBP1, OBP2 and CSP1, respectively, as a single band at approximately 14 kDa, although unspecific bindings occurred at two other proteins around 43 and 66 kDa, respectively **(Fig.3C-E).** The tissue distribution study showed that SguaOBPs specifically expressed in *S. guani* antennae, whereas SguaCSP1 ubiquitously expressed throughout entire tissues tested, including the abdomen, thorax, head, leg, and antennae. At 7.5μg of the total protein loading, SguaCSP1 was the only chemosensory protein detected in both male and female wasps indicating that CSP1 might be more likely to be detected by immunoblotting.

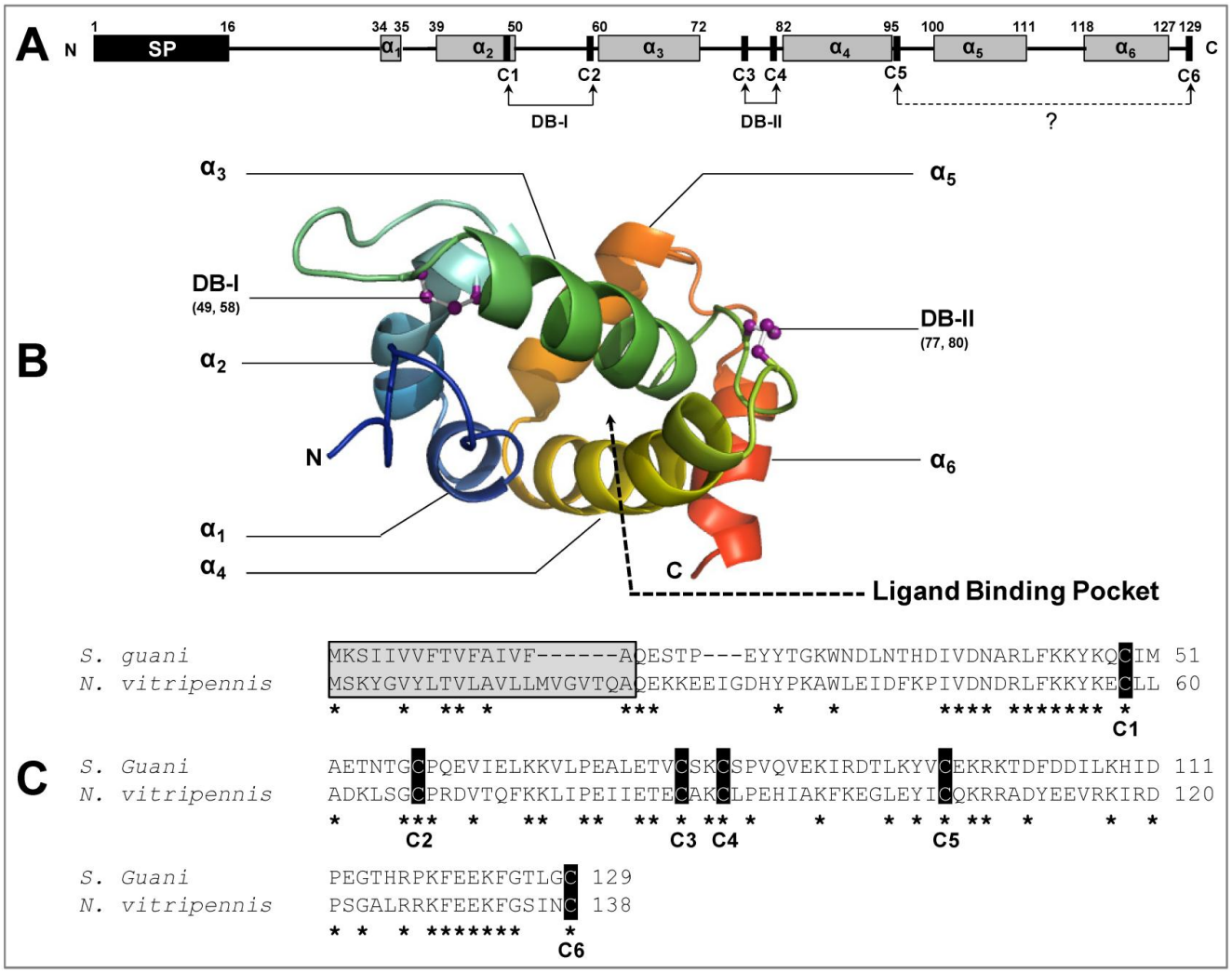

Figure 2. Schematic drawing of three-dimensional structures of *S. guani* CSP. The primary and tertiary structures of Sgua-CSP-1 are depicted in A and B, respectively. Predicted signal peptide (SP) and α-helices are illustrated in black and grey boxes, respectively. A total of six, rather than the typical four, cysteine residues (C1-6) are located in the primary structure of SguaCSP1 (A). Unlike OBP, disulfide bridges (DBs) in CSP are linked by adjacent cysteine residues. However, the structural significance of additional pair of cysteines (C5-6) is unknown (marked with dotted line and question mark). The α-helices, namely α1-6, are color coded in the tertiary structure, and their spatial arrangements are predicted based on the selected protein template from SWISS-MODEL, a web-based protein structure homology-modeling server. N- and C-terminus, disulfide bridges, and the putative ligand binding pocket are highlighted in the simulated SguaCSP tertiary structure (B). So far, only other "Plus-C" type of CSP deposited in the GenBank is from *Nasonia vitripennis* which has the highest sequence identity with Sgua-CSP-1. The peptide alignment (C) shows the six highly conserved cysteine residues (highlighted in black box). Interestingly, the two CSP orthologues have the same cleavage site (Arg-Gln) to separate signal peptides (highlighted in grey box) from mature proteins. Conserved amino acids are denoted with an asterisk. Accession numbers for CSPs used in this study are *S. guani* (ABE68832) and *N. vitripennis* (XP_001601633).

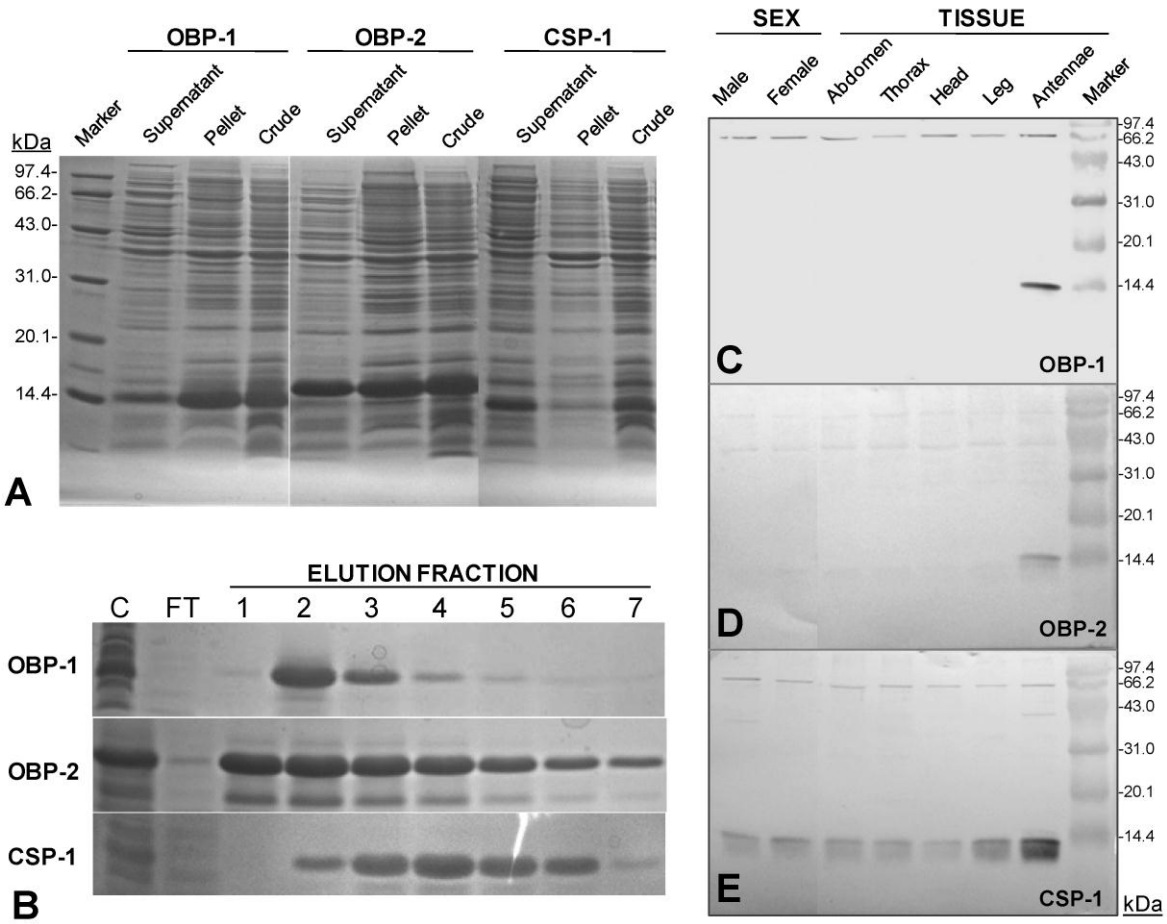

Figure 3. Expression and purification of *S. guani* recombinant olfactory proteins and immunoblot analyses. (A) SDS-PAGE analysis of crude cell lysates prepared before and after the sonication procedure. Recombinant SguaCSP1 exhibited higher solubility than SguaOBPs after sonication under the optimal induction condition (0.4mM IPTG at 25°C for 7h). The resulting supernatant was then purified using a Ni-NTA Superflow Syringe. The elution profiles of recombinant proteins during the purification process were documented by the 15% SDS-PAGE (**B**). C: crude supernatant; FT: flowthrough; and 1-7: elution fractions. (**C-E**) Sex and tissue distribution of OBPs and CSP in adult wasps using immunoblot analyses. SguaOBP1 **(C)** and 2 **(D)** were predominantly detected at the antennae, whereas SguaCSP1 **(E)** expressed ubiquitously across different tissue types including abdomen, thorax, head, leg, and antennae. In addition, CSP1 was more abundant than OBPs in *S. guani* in both sexes.

Gross morphology of *S. guani* antennae

The antennae of *S.guani* are geniculate in shape, and consist of three basic segments: an elongated proximal scape with radicula, a medial pedicel, and a multi-segmented distal flagellum (**Fig. 4C Inset**). Most sensilla were found on the 11-segemented flagellum. There is an apparent sexual dimorphism in relation to antennal sensilla length, type, abundance, and distribution in *S. guani*. Specially, the entire length of antennae is 732.45 ± 20.48μm in females (n=10), and 964.25 ± 25.39μm in males (n=10). The average length of antennal segments in adult males is slightly longer than those of females, with the exception of the scape (**Fig. 4C**). The radicula, the most basal segment of antennae (35.00 ± 4.10μm in females, 42.78 ± 6.13μm in males), connects to the antennal socket where it functions as the fulcrum to the antennae. The scape, the second antennal segment, gradually broadens towards the antennal tip. This is the longest antennal segment in *S.guani* and measures 204.94 ± 10.02μm and 148.60 ± 7.47μm long in females and males, respectively. The shorter, triangular-shaped pedicel (66.90 ± 2.98μm in females, 86.71 ± 4.39μm in males) links the scape to the flagellum. The elongated flagellum is composed of eleven flagellomeres. The first ten flagelomeres do not differ significantly in length, although adult male flagelomeres

are consistently longer than its female counterparts (average length of FI-X: 33.82 ± 2.27μm in females, 56.04 ± 2.63μm in males; Student t-test, n=10, $p<0.001$). The last flagellomere, FXI, is substantially longer than the rest of the flagellum segments (87.39 ± 2.28μm in females, 125.70 ± 5.69μm in males; Student t-test, n=10, $p<0.001$), and has a clava shape which tapers to a circular, flattened point.

Sensilla type

Based on the morphological characteristics, eleven different types of sensilla were documented on the antennae of female and male *S. guani*, including sensilla placodea (SP), long sensilla basiconica (LSB), sensilla basiconica (BS), sensilla coeloconica (SC), two types of double-walled wall pore sensilla (DWPS-I and DWPS-II), two types of sensilla trichodea (ST-I and ST-II), , and three types of sensilla chaetica (SCt-I, SCt-II, and SCt-III). The schematic drawings of the spatial distributions of five antennal multiporous sensilla clearly demonstrate the sexual dimorphism in *S. guani* (**Fig. 4A & B)**. Both LSB and DWPS-I are restricted to the female, whereas the other three types are found on both male and female wasps. The multiporous SP are the largest and most distinctive sensilla type on the antennae for both males and females. The most abundant sensilla, however, are a group of mechanosensilla including sensilla chaetica type II and III. The morphology and fine structure of antennal mechanosensilla (SB, SCt-II and -III) and gustatory sensilla (SCt-I) are described in a companion paper (XL, unpubl. data).

Most of the sensory structures on the 11-segmented *S. guani* flagellum are situated on the medial, upper, and lower surfaces of the nine distal segments, and this distribution pattern is well reflected in the dorsal view of antennal sensilla on the distal-most and penultimate flagellum segments of adult wasps **(Fig. 4D-G)**. The remaining two segments of the flagellum are mostly covered with sensilla chaetica (SCt), a mechanosensilla. In *S. guani*, chemosensilla concentrate on the dorsal side of the flagellum, whereas mechanosensilla are widely distributed among the entire surface of flagellum. This arrangement is observed on all eleven flagellum segments (XL unpubl. data). Based on the external morphology [54] and internal structure [55], the antennal sensilla in *S.guani* were subcategorized into the single-walled multiporous sensilla (SP, LSB, SC, ST-I and ST-II), and the double-walled multiporous sensilla (DWPS-I and DWPS-2). The following are detailed descriptions of the seven chemosensilla in *S.guani*:

Sensilla placodea

Typically, sensilla placodea (SP) have an oval structure with the long axis being parallel to the long axis of the flagellum (**Fig. 4 D, E, F, & G**). At higher magnification (100,000X), numerous wall pores are observed on the surface of SP (**Fig. 5A&B**). However, as shown in both scanning electron micrographs and transmission electron micrographs, there are subtle differences in the shape of this sensory organ between males and females. The SP cuticular walls (approximately 0.21μm in male, 0.55μm in female) are generally thinner and slightly elevated in the male flagellum (**Fig. 4 D & E; Fig. 5C**) in comparison to the female flagellum (**Fig. 4 F & G**, **Fig. 8L**).

Long sensilla basiconica

These sensilla are exclusively found on most flagellum sub-segments of female *S.guani*, and their spatial arrangement follows a specific pattern (**Fig. 4B**). The last section of the female flagellum (FXI) has six LSB with a 2:4 linear arrangement (**Fig. 4B)**. A pair of LSB is consistently observed at the distal portion of each flagellomere between FVI to FX, whereas only one LSB exists on FIV and FV. LSB are absent from the remaining flagellomeres. In general, LSB have a thumb-like shape and are characterized by a grooved surface (**Fig. 5 F&G)**, which projects perpendicularly with respect to the axis of *S.guani* antennae (**Fig. 5F**). Multiple wall pores are clearly visible on the ventral surface of the thumb tip based on the scanning electron micrograph (**Fig. 5G**). The transmission electron micrograph shows a thin multiporous cuticular wall surrounded an inner lumen innervated by more than twenty dendritic branches (**Fig. 5H & Fig. 8A**).

Sensilla coeloconica

Sensilla coeloconica (SC) are characterized by short pegs, with a juglans-shape and a deep grooved head and a short smooth surface stem, which is located in deep depressions surrounded by a clock-shaped ring (**Fig. 5D & Fig.7D**). SC are found on both male and female flagellomeres (male - FXI and VIII, female - FXI, X, IX, and VII) with only one SC for each segment (**Fig 4A&B**). Ultrathin sections of the internal postpedicel of the SC show a thick, nonporous sensillum wall, and two branched dendrites which are immersed in the central lumen (**Fig. 5E**).

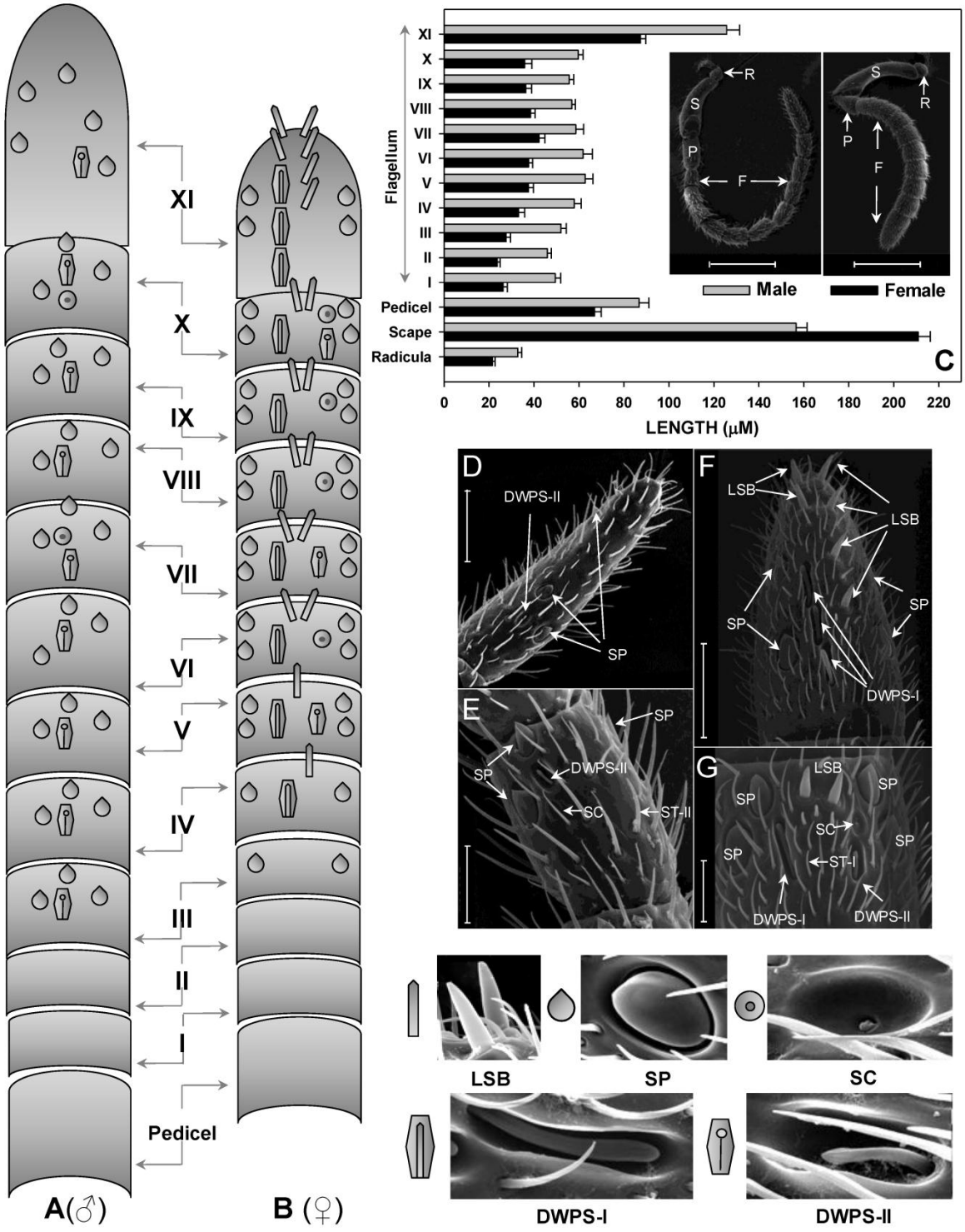

Figure 4. Abundance and distribution of chemosensitive sensilla on *S. guani* antennae. Schematic drawings of spatial distributions of five chemosensitive sensilla including Sensilla Placodea (SP), Long Sensilla basiconica (LSB), Sensilla Coeloconica (SC), Double-walled Wall Pore Sensilla Type I (DWPS-I), and Double-walled Wall Pore Sensilla Type II (DWPS-II) on 12-segmented flagellum are presented in both male **(A)** and female **(B).** The average lengths of antennal segments among adult males and females are summarized in **(C).** The lengths of segments of adult male are slightly longer than those of the female, with the exception of the scape. **C-Inset** shows that both female and male *S.guani* have serrated flagellar antennae which consist of scape (S), pedicel (P), and flagellum (F). The distribution and arrangement of various antennal sensilla on the distal-most (FXI) and penultimate (FX) flagellum segments were visualized in male **(D&E)** and female **(F&G)**, respectively, using a scanning electron microscope (SEM). ST: Sensilla Trichodea. Scale bars: Scale bars: D=43μm, E=23.1, μm F=30μm, G=13.6μm.

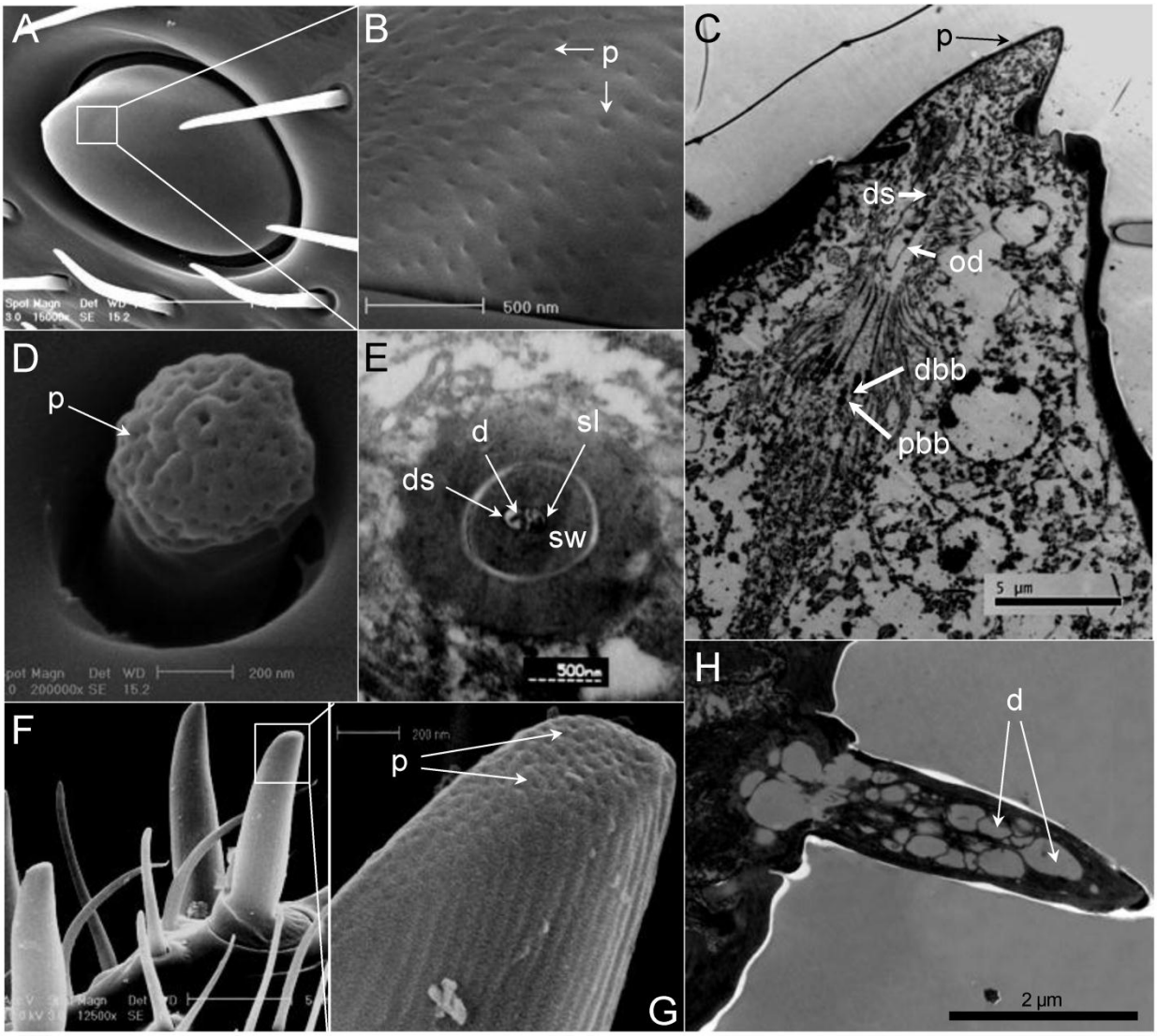

Figure 5. Single-walled multiporous sensilla. (A) Sensilla Placodea (SP). **(B)** Close-up of **A** showed numerous wall pores (p) on the surface of SP. **(C)** Longitudinal section of SP. Six pairs of distal basal body (dbb) and proximal basal body (dbb) can be identified. The expand outer dendrites (od) with dendritic sheath (ds) stretch to the end of plate surface. **(D)** Sensilla Coeloconica (SC). **(E)** Transverse section through proximal end of SC. Two dendrites (d) which immerse in sensillum lymph (sl) are surrounded by a thick sensilla wall (sw). **(F)** Long Sensilla basiconica . **(G)** Close-up of **F** shows numerous wall pores (p) on the tip of LSB surface. **(H)** Longitudinal section of LSB. Scale bars: A=5µm, B=500nm, C=5µm, D=200nm, E= 500nm, F=5µm, G=200 nm, H=2µm.

Sensilla trichodea

The entire antennal segments of both male and female are abundantly covered with sensilla trichodea (ST). In general, these blunt end hair structures are inclined and slightly curved toward the apex of the segment, but show different external structures between the male (ST-II) and female (ST-I). In female antennae, type-I ST (ST-I) exhibits longitudinal grooves that parallel its vertical axis surface (**Fig. 6 D&E**). In male antennae, type-II ST (ST-II) have smooth surfaces with fewer pores than females (**Fig. 6 A&B**). Based on the transmission electron micrograph, both types of ST have thin cuticular walls with multiple pores on their surfaces (**Fig. 6 C & F, and Fig 8C**).

Double-walled multiporous sensilla

Two types of double-walled multiporous sensilla, namely double-walled wall pore sensilla type I (DWPS-I) and type II (DWPS-II), are observed in females (**Fig. 4**), but only one type occurs in males (**Fig.**

4A). DWPS-I is found in both males (**Fig. 4A, D&E**) and females (**Figs. 4B, F&G**), whereas DWPS-II exists only in females (**Figs. 4B, F&G**).

DWPS-I has a finger shape with longitudinal grooves, fluted aporous walls, and a stem base plug in a deep hole of the antenna; the entire sensillum is surrounded by a barbell chamber (**Fig.7A**). A cross-section at the basal position of DWPS-I shows a single dendrite indicating that a single neuron enervating the sensillum (**Fig. 7C**), whereas a cross-section at the distal position exhibits one large unbranched and fourteen branched dendrites which are immersed in the sensillum lymph enclosed by the double-walled cuticular fingers (**Fig. 7B**).

DWPS-II has an expanded head with grooves and a long smooth stem plug in a deep hole which is surrounded by a barbell chamber (**Fig. 7D**). There are fewer pores hidden on the grooves (**Fig. 7E**). Cross-section profiles through the distal part to the base part of the sensory structure appear much more complex than DWPS-I. Cross sections close to the peg tip shows that the five partially fused cuticular fingers appear to surround the central lumen (**Fig. 8H**). More distally, the numbers of dendrites as well as the cuticular fingers increase. A cross-section of the distal section shows twelve cuticular fingers surrounding the central lumen, in which three dendrites are visible (**Fig. 7E**). The cross-section through the basal, unscalloped part of the peg shows the double-walled structure. The peripheral lumen between the two cuticular walls is completely filled with electron-dense tubules; three outer dendritic segments are surrounded by the inner cuticular wall (**Fig.7F**).

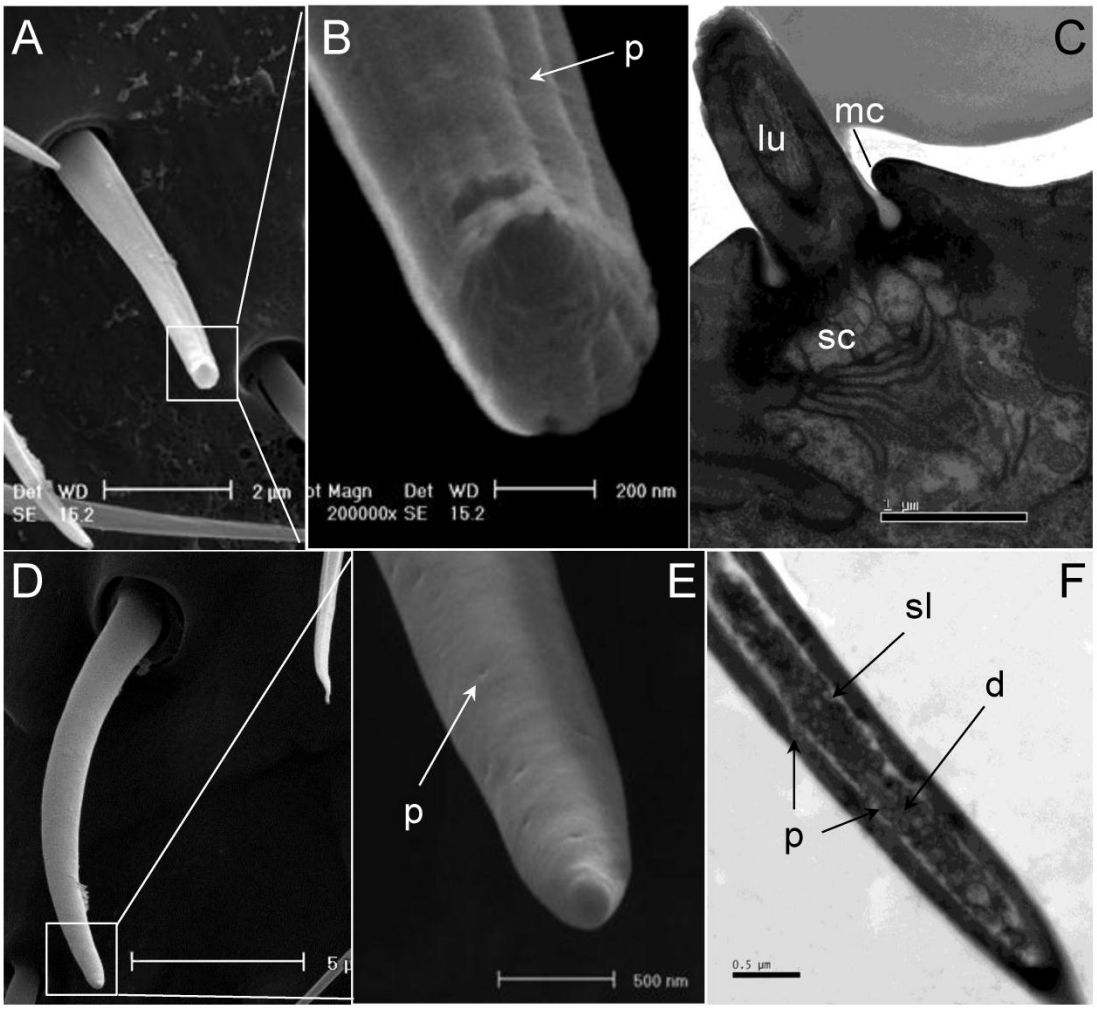

Figure 6. Sensilla trichodea. (A) Scanning electron micrograph of sensilla trichodea (ST) on female antennae. **(B)** Close-up of **A** shows shallow grooves and wall pores on the cuticular wall. **(C)** Longitudinal section of ST on female antennae. **(D)** Scanning electron micrograph of ST on male antennae. **(E)** A smooth surface and wall pores are observed on the surface of male ST. **(F)** Longitudinal section of ST on male antennae. lu: lumen of hair, mc: molting channel, sc: socket cavity. Scale bars: A=2µm, B=200nm, C=1 µm, D=5µm, E=500nm, F=0.5 µm.

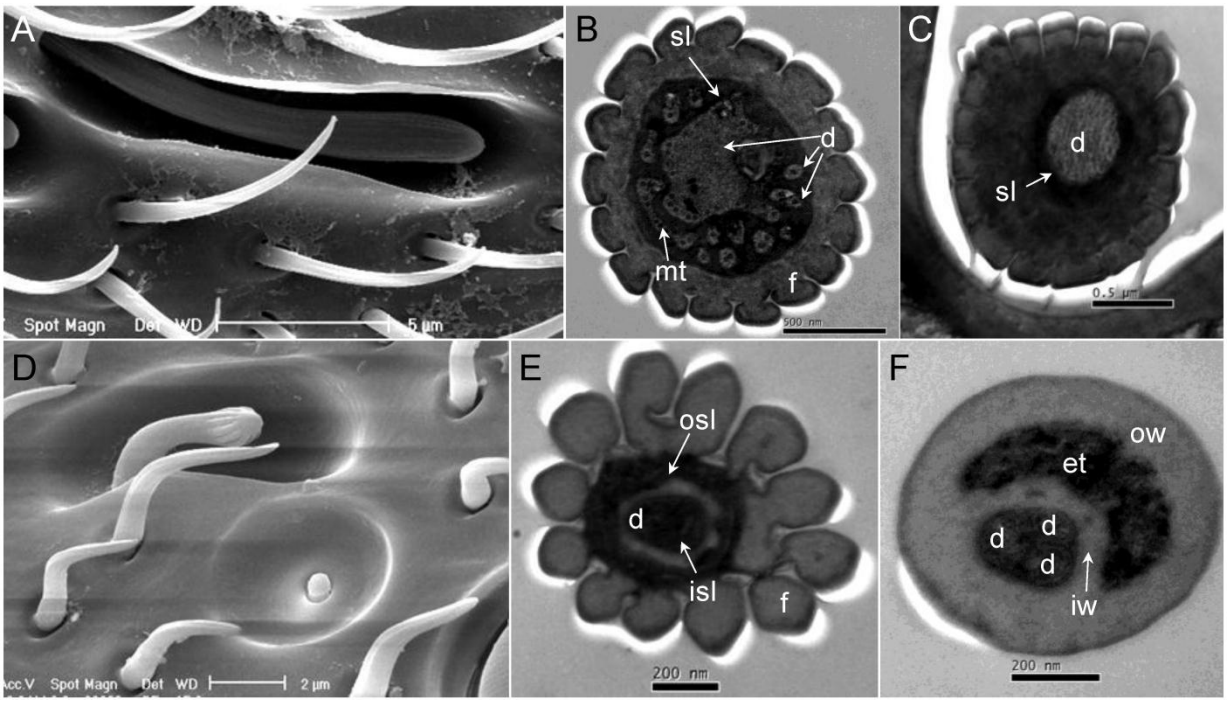

Figure 7. Double-walled multiporous senslilla. (A) Double-walled Wall Pore Sensilla Type-I (DWPS-I**). (B)** Transverse cross-section at the distal level of DWPS-I. A total of fifteen branched dendrites are immersed in the sensillum lymph cavities (sl). mt: micro tube. **(C)** Transverse cross-section at the basal level of DWPS-I. The sensillum lymph cavities (sl) contain a single unbranched dendrite. **(D)** Double-walled Wall Pore Sensilla Type-II. **(E)** Transverse cross-section at the distal level of DWPS-II. **(F)** Transverse cross-section at the basal level of DWPS-II. The sensillum lymph cavities (sl) contain three branched dendrites. isl: inner sensillum lymph, osl: outer sensillum lymph, f: cuticle finger, iw: inner cuticular wall, ow: outer cuticular wall, et: electrondense tubules. Scale bars: A=5µm, B=500nm, C=0.5 µm, D=2µm, E=200nm, F=200nm.

Immunolocalization of SguaOBP1, OBP2 and CSP1 on antennal sensilla

The antiserum raised against SugaOBP1 labeled LSB, ST-I, ST-II and SP. In LSB, the gold granules are very concentrated in the sensillum lymph bathing numerous dendrites **(**dilution of primary antibody at 1:1000, **Fig. 8B).** The cross-section of the basal portion of the ST-II is heavily labeled, and gold granules are widely distributed throughout the sensillum lymph (dilution of primary antibody at 1:1000, **Fig 8F**). ST-I are moderately stained under a lower concentration of antiserum **(**dilution of primary antibody at 1:6000, **Fig. 8D)**. SP are moderately labeled by anti-OBP1 and gold granules are restricted at wall pores and the molting channels (dilution of primary antibody at 1:6000, **Fig. 8G**). The antiserum raised against SguaOBP2 specifically labels DWPS-II. The gold granules are very concentrated at the sensillum lymph as well as the wall pores (dilution of primary antibody at 1:3000, **Fig. 8I**). Antiserum raised against SguaCSP1 (dilution of primary antibody at 1:6000) labels DWPS-I (**Fig. 8K)**, SP (**Fig. 8M**), and SC (not shown). The gold granules are predominately concentrated in the sensillum lymph surrounding the dendrite sheath with various levels of intensity. In addition, the cuticle and dendrites of all sensory hairs are not labeled by any antiserum. The labeling patterns of adult males and females are similar.

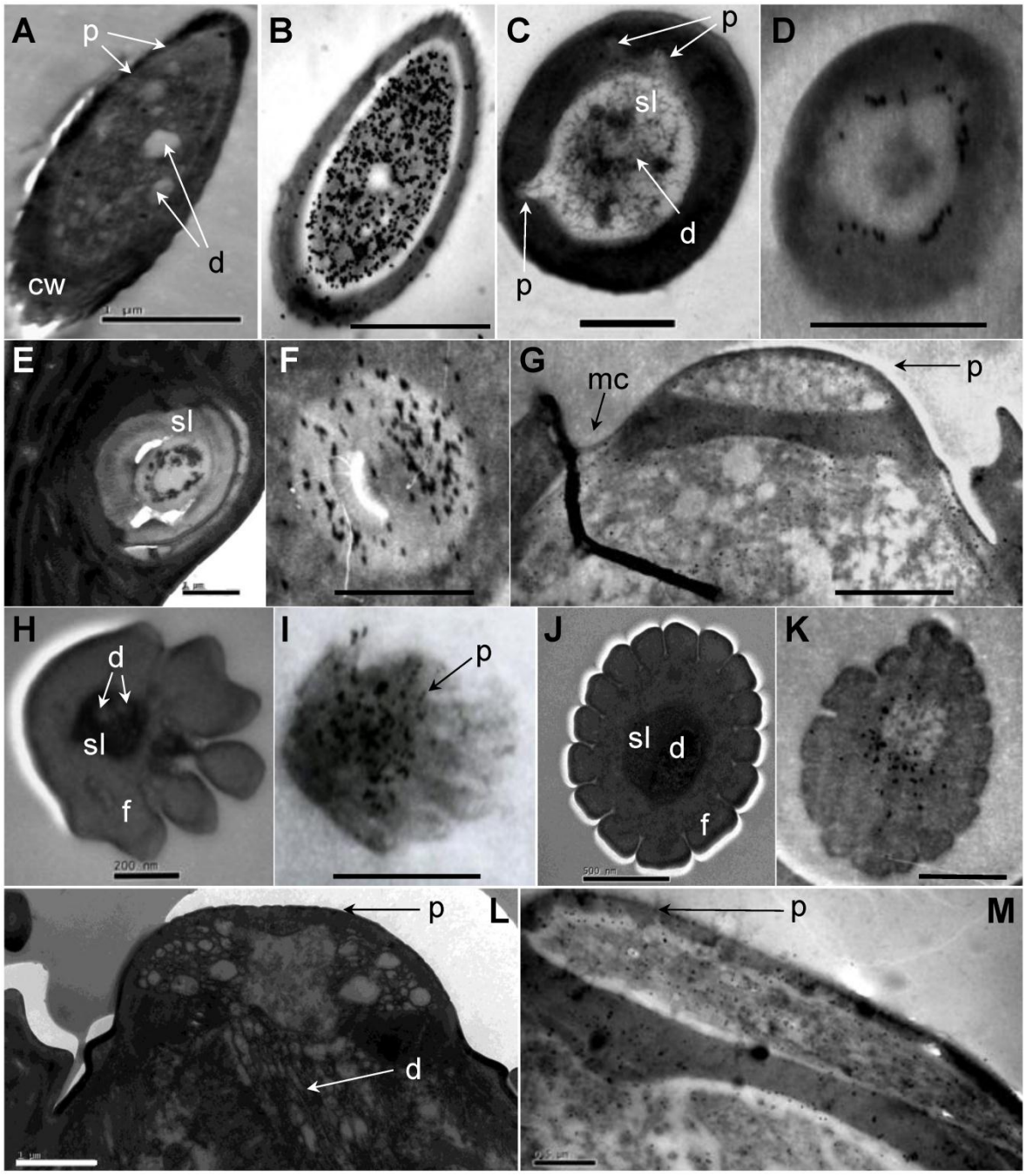

Figure 8. Immunolocalization of chemosensitive sensilla on *S. guani* antennae. (A) Transverse cross-section of LSB. **(B)** LSB shows strong labeling with anti-OBP1. (C) Transverse cross-section of ST-I. **(D)** ST-I are moderately labeled with anti-OBP-1, but gold granules are restricted to the sub-cuticular space around the sensillum lymph (sl). **(E)** The cross-section of the basal portion of the ST-II. **(F)** anti-OBP1 is widely distributed throughout the sensillum lymph (sf) of ST-II. **(G)** SP are moderately labeled by anti-OBP1, and gold granules are restricted at wall pores (p) and molting channels (mc). **(H)** Transverse cross-section of DWPS-II. **(I)** DWPS-II are specifically labeled with anti-OBP2. The gold granules are concentrated at the sensillum lymph (ls) as well as the wall-pores. **(J)** Transverse cross-section of DWPS-I. **(K)** DWPS-I are heavily labeled with anti-CSP1. The gold granules are exclusively located at the outer sensillum lymph (osl) cavity without dendrites, but not in the inner sensillum lymph (isl) cavity. **(L)** Longitudinal cross-section of SP. **(M)** SP are labeled with anti-CSP-1in sensillum lymph (sl) and wall pores (p). Scale bars: A=1μm, B=1μm, C=1 μm, D=500nm, E=1 μm, F=1 μm, G=1.4 μm, H=200nm, I=833nm, J=500nm, K=500nm, L=1μm, M=0.5μm.

Discussion

Structural significance of SguaOBP and CSP

The presence of conserved cysteines is a typical feature of OBPs and CSPs. Xu *et al* [44] developed a suite of conserved C-patterns to search for novel OBPs and CSPs in the existing large scale EST database, and authors successful identified 142 OBPs and 177 CSPs, of which 117 OBPs and 129 CSPs are new. With the advent of Genomic Era, C-patterns have been quickly adopted to annotate the OBPs and CSPs from newly resolved insect genomes or high-throughput EST datasets [44, 56-58]. Given the fact that there are no apparent differences in C-patterns of OBPs and CSPs across different insect Orders, the utility of C-patterns in the genome annotation is extremely promising.

Based on the C-pattern (number of conserved cysteine residues), insect OBPs have been further categorized into: Classic OBPs (one six-cysteine motif), Dimer OBPs (two six-cysteine motifs), Plus-C OBPs (eight-cysteine motif plus one proline), Minus-C OBPs (four-cysteine motif), and Atypical OBPs (9-10 cysteines plus a long C-terminus) [45]. It is worth noting that these non-classical OBPs (Dimer OBPs, Plus-C OBPs, Minus-C OBPs, and Atypical OBPs) are not uncommon among insects, and they are not restricted to particular taxa. For instance, among the 72 putative OPBs annotated from the *Anopheles gambiae* genome, almost half of them belong to non-classical groups (37 classic and 35 non-classic OBPs; [45]). In congruence with previous motif analyses [44, 45], C-pattern in SguaOBPs and CSP are highly conserved. In this study, the C-pattern of OBPs from *S. guani* is consistent with the classic cysteine motif proposed by Xu *et al* [44] for Hymenoptera. In the case of SguaCSP1, however, the c-pattern is clearly deviated from the highly conserved classic CSP cysteine motif. Based on the naming system for insect OBPs, this new group of CSPs is designated as a Plus-C CSP.

The structural significance of the signature cysteine motif in OBPs is to form disulfide bridges to maintain the integrity of their three-dimensional structures [24, 42, 45, 59]. In CSPs, however, disulfide bridges formed by the conserved cysteines are believed to not directly associate with the stability of the 3-D CSP structures [24, 45, 60]. However, the three-dimensional structure of a Plus-C CSP predicted in this study will add new information to a seemly highly conserved four-cysteine signature motif in CSP, and may potentially challenge the contention that these conserved cysteines are irrelevant to the stability of CSP tertiary structure. In classic CSPs, disulfide bridges are formed by the adjacent cysteine residues and the distances between the linked cysteine pairs never exceed eight amino acids [44]. The distance between C5 and C6 in SguaCSP1 primary structure, however, is 33 amino acids, although C5 and C6 are in a close proximity in the tertiary structure. Insect OBPs and CSPs are helical structures and typically follow their respective folding patterns. The major conformational differences, however, mainly occur at the N and C-terminal regions. These terminal regions interact with ligand molecules directly, and the differences in these end regions may dictate the ligand binding specificity and may also impact the entry and release mechanisms of ligand molecules. In comparison to the classic CSPs, the Plus-C SguaCSP1 may have evolved additional binding capacity because the additional cysteine pair is on the C-terminal region with C6 occupying the C-terminus. The structural significance of this additional cysteine pair warrants further investigation.

It is also worth noting that the primary structure of SguaCSP1 comprises of 12 Glu, 8 Asp, 14 Lys, and 4 Arg residues, accounting for 33.6% of the CSP mature protein. All of these charged residues are located at the peptide surface, and this particular structural configuration makes SguaCSP1 extremely water soluble. The high solubility of SguaCSP1 is reflected in the recombinant protein expression experiment **(Fig. 3A)**.

Tissue distribution of SguaOBP and CSP

Generally, OBPs are considered to be antenna-specific, whereas CSPs are widely distributed throughout the body, including the head, antennae, proboscis, thorax, legs, sub-cuticular epithelium, pheromone glands, and ejaculatory duct [39]. However, an antenna-specific CSP has been reported in the Argentine ant [61]. Calvello *et al* [38, 62] also reported an antenna-specific CSP, as well as an OBP expressed in legs and wings in the wasps, *Polistes dominulus* and *Vespa crabro*. In agreement with previous reports, SguaOBPs specifically expresses in the *S. guani* antennae, whereas SguaCSP1 is ubiquitously distributed throughout different tissues, including the abdomen, thorax, head, leg, and antennae. The broad distribution of CSPs in various organs and tissues has direct functional implications. Other than a lipid carrier, CSPs are believed to be involved in the production, release, and reception of pheromones in *Lepidoptera* [63, 60], and in Blattaria, a CSP is even involved in leg regeneration [64].

In nature, the operational sex ratio in *S. guani* is biased toward females (17 to 1 female to male ratio). Males only survive for several days with a sole purpose of mating [1]. In contrast, female wasps live much longer and have a full range of behaviors which

demand chemosensory supports. The immunoblot analyses with different sexes show that OBPs and CSP are differentially expressed in males and females. Specifically, SguaOBPs are absent from males, whereas SguaCSP1 presents in both males and females. Possibly, the discrepancy in the expression patterns of SguaOBP and CSP in male and female *S. guani* is the direct result of their distinctive life styles.

S. guani antennal sensilla and its relationship with other *Hymenoptera parasitoids*

Seven multiporous chemosensilla including sensilla placodea (SP), long sensilla basiconica (LSB), sensilla coeloconica (SC), two types of double-walled wall pore sensilla (DWPS-I and DWPS-II), and two types of sensilla trichodea (ST-I and ST-II) are reported in this paper. Many of these antennal sensilla have been described in other parasitic wasps, although nomenclature used in some of these studies was not consistent. Based on the original descriptions, the distribution patterns of seven antennal sensilla including sensilla placodea (SP), sensilla trichodea (ST), sensilla basiconica (BS), sensilla coeloconica (SC), sensilla chaetica (SCt), sensilla styloconica (SS), and campaniform sensilla (CS) are compared in twenty Hymenoptera parasitoid species, including four ectoparasitic (**Table 1)** and sixteen endoparasitic wasps **(Supplementary Material: Table S2**).

Table 1. Diversity of antennal sensilla in Hymenoptera ectoparasitoids

Parasitoid Species	Family	Function[1]	Sensilla Type		Reference
			Sensilla[2]	Pore[3]	
Scleroderma guani	Bethylidae	Ectoparasitoid (generalist, larvae)	SP	M	This study
			ST-I,II	M	
			LSB	M	
			SB	A	
			DWPS-I, II	M	
			SC	M	
			SCt-I	U	
			SCt-II, III	A	
Pteromalus cerealellae	Pteromalidae	Ectoparasitoid (generalist, larvae)	SP	M	[18]
			ST-I, II, IV	A	
			ST-III	M	
			SB	A	
			SC	A	
			SCt	U	
Spathius agrili Yang	Braconidae	Ectoparasitoid (specialist, larvae)	SP	M	[22]
			ST-I	M	
			ST-II	A	
			SS	M/U	
Tamarixia radiata	Eulophidae	Ectoparasitoid (specialist, nymph)	SP	M	[20]
			ST-I, II	A	
			ST-III	M	
			SB	A	

"1": The potential biological control functions of the listed parasitoids.

"2": Types of antennal sensilla, including sensilla placodea (SP), sensilla trichodea (ST), sensilla basiconica (SB), long sensilla basiconica (LSB), sensilla coeloconica (SC), sensilla chaetica (SCt), sensilla styloconica (SS), campaniform sensilla (CS), and double-walled wall pore sensilla (DWPS).

"3": Types of antennal sensilla based on the presence or absence of pore (s), including multiporous sensilla (M), uniporous sensilla (U), and aporous sensilla (A).

Among these sensilla, SP is by far the most common type which appears on the antennae of each Hymenoptera parasitoid species surveyed, although in various sizes and shapes. In most parasitic wasps, SP are elongated in shape and arranged in alternate rings around the antennomeres. In this study, both male and female *S. guani* have SP. However, the external structure of SP in *S. guani* is different from the

classic shape observed in other parasitic wasps, except for *Gryon gallardoi* (Brèthes), an egg parasitoid (it was referred to as papillary sensilla in Rocha *et al* [16]. These pore plate structures have a somewhat oval structure with their long axis being parallel to the long axis of the flagellum. The closest resemblance of this type of SP has been found in honeybees, Apis mellifera adansonii [65] and Apis mellifera ligustica (Spinola) [66].

Following SP (100%), ST (84.2%), BS (68.4%), SCt (57.8%), and SC (52.6%) are fairly common among the surveyed parasitoids, whereas SS (15.8%) and CS (5.3%) are the least abundant sensilla in parasitic wasp. As the second most abundant sensilla, ST have a hair or peg like structure, with multiple, one, or no pores on the wall. In *S. guani*, there are two types of mutilporous ST. The differences between them are, ST-I are characterized by the parallel grooved walls whereas ST-II have smooth walls. BS have a thicker body than that of ST, with multiple pores on sensilla tips [13] or around the walls [13, 12]. In some cases, BS are aporous. In our study, there are two types of SB, including the long basiconica sensilla with a tip and wall pores, and the aporous basiconica sensilla. Half of SC are aporous sensilla [18, 21] and the other half are uniporous senlilla [12]. In *S. guani*, however, SC have a multiporous structure. In this study, two types of DWPS are identified in *S. guani*, and they both have double wall structure with pores resided in deep grooves. The cross-section profiles of these sensilla are similar to the double-walled wall pore sensilla (DW-WP) in the *Carausius morosus* [67].

In parasitic hymenopterans, antennal sensilla are specialized to carry out the functions of habitat searching, host localization, recognition, selection, and acceptance, and oviposition, courtship and mating behavior [21, 68]. When a female parasitoid emerges and seeks out the preferred habitat, normally she uses her antennae to sense host chemical cues. From this host selection process, it appears that antennae play a fundamental role in detecting various semiochemicals, either volatiles acting as attractants, or nonvolatiles acting on contact [68]. Among the ectoparastic wasps surveyed in **Table 1**, all four of them are larval parasitoids, and represent four distinct Hymenoptera families. The diversity of the sensilla type is related to host specialization. *Scleroderma guani* (Hymenoptera: Bethylidae) and *Pteromalus cerealellae* (Hymenoptera: Pteromalidae) are highly polyphagous generalists, whereas *Spathius agrili* Yang (Hymenoptera: Braconidae) and *Tamarixia radiate* (Waterston) (Hymenoptera: Eulophidae), are monophagous specialists. *Spathius agrili* is a gregarious ectoparasitoid of the emerald ash borer, *Agrilus planipennis* Fairmaire (Coleoptera: Buprestidae), an exotic invasive wood-boring beetle that is a serious threat to ash trees throughout North America. *Tamarixia radiate* is an effective ectoparasitoid of the Asian citrus psyllid, *Diaphorina citri* Kuwayama (Hemiptera: Psyllidae), one of the most devastating insect pests of citrus worldwide. The diversity of sensilla type in generalists is much higher than that of specialist. More than five major types of sensilla functioning as either chemo- or mechano-receptors have been identified on the antennae of *S. guani* (11 subtypes) and *P. cerealellae* (8 subtypes), respectively. In contrast, *S. agrili* and *T. radiate* have only three major sensilla types. The broad host range and complex host-parasitoid interactions require sufficient sensory supports from sensory organs like antennae and would likely be related to the more diverse sensilla types observed in the generalist parasitoids.

Immunolocalization profiles of SguaOBPs and CSP

Each sensillum immunoreacts with at least one plolyclonal antiserum raised against respective recombinant SguaOBPs and CSP **(Table 2)**. Anti-OBP2 is the most specific antibody and can only be labeled in the sensillum lymph of DWPS-II. On the contrary, anti-OBP1 shows a broad spectrum of immunoactivity toward four different sensilla, including LSB, SP, ST-I and ST-II. The immunolocalization profiles between two OBPs could be the reflection of their structural differences, and suggests different chemosensory functions, i.e., SguaOBP1 and 2 bind different ligands which lead to different chemosensory pathways and result in different biological functions (e.g., behavior). The predicted three-dimensional structure shows a similar folding for these two proteins **(Fig. 1C & D)**. The spatial organization of the six helical structures of SguaOBP1 and 2 is very consistent. The major difference, however, is at the C-terminal region in which SguaOBP2 has a prolonged C-terminal region (21 amino acids away from helix α6) in comparison to SugaOBP1 (6 amino acids away from helix α6). These structural predictions, however, are not sufficient to determine if such terminal differences lead to different ligand specificities. Ligand binding assays and a better resolution of the three-dimensional structure, especially the ligand binding pocket for these two SguaOBPs, would be necessary to definitively determine the binding specificity and function of these two OBPs.

On the other hand, anti-CSP1 is fairly immunoactive toward both SP and DWPS-I, and shows weak binding capability with SC. It is not surprising to see the different immunolocalization profiles between the OBP and CSP because these two share no sequence

similarity. Intriguingly, however, it's the observation of a cross co-localization of anti-OBP1 and anti-CSP1in *S. guani* SP, the most abundant antennal sensilla in the Hymenoptera parasitic wasps. The phenomenon of co-localization was first discovered in *Drosophila* for OS-E and OS-F [69] and LUSH [70], and later in moths [71]. So far, the co-localization phenomenon has been documented strictly within the OBP-GOBP family, and this report is the first observation of the cross co-localization between OBPs and CSPs.

Table 2. Immunolocalization of OBPs and CSP in antennal sensilla of *S. guani*

Sensilla Type*	Anti-SguaOBP1	Anti-SguaOBP2	Anti-SguaCSP1
LSB	+++**	-	-
SP	++	-	+++
SC	-	-	+
DWPS-I	-	-	+++
DWPS-II	-	+++	-
ST-I	+++	-	-
ST-II	++	-	-

"*": Antennal sensilla types in *S. guani*, including long sensilla basiconica (LSB), sensilla placodea (SP), sensilla coeloconica (SC), double-walled wall pore sensilla type I and II (DWPS-I & II), sensilla trichodea type I and II (ST-I & II) .

"":** Positive labeling with the respective antibody is shown by "+", whereas "-"represents background labeling only. The labeling intensity (+++ strong, ++ intermediate, + weak) is arbitrarily determined based on the distribution pattern of gold granules hybridized to the target sensilla. Specifically, the strong labeling denotes a broad distribution of gold granules throughout the sensillum lymph, the intermediate labeling represents a peripheral or restricted distribution pattern, and the weak labeling defines a sparsely distributed pattern which is above the background labeling level.

Summary

In silico structural analyses indicate that the SguaOBP1 and 2 are classic OBPs with a signature six-cysteine C-pattern and a similar tertiary structure. The structural modification at the C-terminal region (e.g., prolonged C-terminal region in SugaOBP2), however, may differentiate the binding specificity with olfactory ligands between the two OBPs. The different immunolocalization profiles of SugaOBP1 and 2 clearly reflect such binding discrepancies. SguaCSP1, on the other hand, belongs to a non-classic CSP group with two additional cysteine residues downstream of the classic four-cysteine motif. Currently this "Plus-C" type has only been found in two ectoparasitoids, *S. guani* and *N. vitripennis*. In comparison to the classic CSPs, the structural significance of an additional pair of cysteine residues on the C-terminal region is extremely intriguing. The spatial arrangement of C5 and C6 is more like an "interlock" rather than the conventional "adjacent" pattern, and the resulting disulfide bridge may challenge the "relaxed" structural model for the classic CSPs. A refined three-dimensional structure of SugaCSP1 using X-ray crystallography and ligand binding assays will be necessary to elucidate the structural and functional significance of this newly discovered non-classic Plus-C CSP group.

Eleven types of sensilla are found in the flagellum and pedicel segments of antennae in both male and female wasps, seven of which are multiporous chemosensilla and their ultrasturctures are morphologically characterized in this report. In addition, antennal sensilla types from *S. guani* are compared with nineteen other *Hymenoptera parasitoids including both endo- and ecto-parasitoids*. In ectoparasitic hymenopterans, the diversity of sensilla types is apparently a reflection of the different biological functions provided by the polyphagous or monophagous parasitoids. The immunocytochemistry study correlates the *S. guani* olfactory proteins with their respective sensilla. Anti-OBP2 is highly specific whereas anti-OBP1 shows a broad spectrum of immunoactivity toward four different types of sensilla. The structural difference at the C-terminal region between SguaOBP1 and 2 may contribute to this binding discrepancy. Interestingly, a cross co-localization pattern between OBP and CSP is documented for the first time. Given the fact that 51 OBPs and 4 CSPs from *Drosophila melanogaster*, 44 OBPs and 18 CSPs from *Bombyx mori*, and 46 OBPs and 20 CSPs from *Tribolium castaneum* [72] potentially reside on limited types of sensilla from each species, it is possible that such phenomenon could be the rule rather than the exception.

Acknowledgments

The authors are grateful to Drs. Kenneth Haynes and John Obrycki (University of Kentucky) for their comments on an earlier draft. Special thanks go to Fei Sun (Chinese Agricultural University) for the technical assistance and three anonymous reviewers for their critical comments and suggestions. This research was supported by the China National Basic Research Program (973 Project) of Invasion Biology and Control Strategies for Alien Species in Agriculture and Forestry (Award number: 2002cb111407).

Supplementary Material

Table S1. Primer sequences for recombinant SguaOBP1, OBP2, and CSP1.
Table S2. Diversity of antennal sensilla in Hymenoptera endoparasitoids.
http://www.biolsci.org/v07p0848s1.pdf

Author Contribution

XRL conceived the entire experiments; XRL, DL, QZ, and XZ designed the study; XRL, XXL, and XZ analyzed the data; and XRL and XZ wrote the manuscript. All authors read and approved the final version of manuscript.

Conflict of Interests

The authors have declared that no conflict of interest exists.

References

1. Chen J, Cheng H. Advances in applied research on Scleroderma spp. (in Chinese). Chin J Biol Con. 2000; 16: 166-170.
2. Ding Y, Lu C, Han B, et al. Relationship between growth potential of pine, population density of Monochamus alternatus and pathogenicity of Bursaphelenchus xylophilus (in Chinese). Chinese J Applied Ecolo. 2001; 12: 351-354.
3. Shi J, Luo Y, Wu H, et al. Impact of the invasion by Bursaphelenchus xylophilus on forest growth and related growth models of Pinus massoniana population. Acta Ecologica Sinica. 2008; 28:3193-3204.
4. Xu F, Xu K, Xie C, et al. Studies on the Scleroderma guani Xiao et Wu to control the pine wood nematodes. In: Mota M, Vieira P, ed. Pine wilt disease: a worldwide threat to forest ecosystems. The Netherlands: Springer; 2008; 51-52.
5. Hu J, Angeli S, Schuetz S, et al. Ecology and management of exotic and endemic Asian longhorned beetle Anoplophora glabripennis. Agr Forest Entomol. 2009; 11: 359-375.
6. Haack RA, Hérard F, Sun J, et al. Managing invasive populations of Asian longhorned beetle and citrus longhorned beetle: a worldwide perspective. Ann Rev Entomol. 2010; 55: 521-546.
7. Altner H, Prillinger L. Ultrastructure of invertebrate chemo-, thermo-, and hygroreceptors and its functional significance. Int Rev Cytol. 1980; 67: 69-139.
8. Zacharuck R. Antennae and sensilla. In: Gilbert LI, Kerkut GA, ed. Comprehensive Insect Physiology, Biochemistry and Pharmacology, v6. Oxford: Pergamon Press; 1985: 1-70.
9. McIver SB. Mechanorreception. In: Kerkut GA, Gilbert LI, ed. Comprehensive insect physiology biochemistry and pharmacology, v6. Oxford: Pergamon Press; 1985:71-132.
10. Amornsak W, Cribb B, Gordh G. External morphology of antennal sensilla of trichogramma australicum girault (Hymenoptera: Trichogrammatidae). Int J Insect Morphol Embryol. 1998; 27: 67-82.
11. Baaren J van, Boivin G, Lannic J Le, et al. Comparison of antennal sensilla of Anaphes victus and A. listronoti (Hymenoptera, Mymaridae), egg parasitoids of Curculionidae. Zoomorphology. 1999; 119: 1-8.
12. Cônsoli FL, Kitajima EW, Parra JR. Sensilla on the antenna and ovipositor of the parasitic wasps Trichogramma galloi Zucchi and T. pretiosum Riley (Hym., Trichogrammatidae). Microsc Res Tech. 1999; 45: 313-324.
13. Le Rü B, Renard S, Allo M-R, et al. Antennal sensilla and their possible functions in the host-plant selection behaviour of Phenacoccus manihoti (Matile-Ferrero) (Homoptera : Pseudococcidae). Int J Insect Morphol Embryol. 1995; 24: 375-389
14. Bleeker MA, Smid HM, van Aelst AC, et al. Antennal sensilla of two parasitoid wasps: a comparative scanning electron microscopy study. Microsc Res Tech. 2004; 63: 266-273.
15. Roux O, van Baaren J, Gers C, et al. Antennal structure and oviposition behavior of the Plutella xylostella specialist parasitoid: Cotesia plutellae. Microsc Res Tech. 2005; 68: 36-44.
16. da Rocha L, Moreira GR, Redaelli LR. Morphology and distribution of antennal sensilla of Gryon gallardoi (Brèthes) (Hymenoptera: Scelionidae) females. Neotrop Entomol. 2007; 36: 721-728.
17. Gao Y, Luo LZ, Hammond A, et al. Antennal morphology, structure and sensilla distribution in Microplitis pallidipes (Hymenoptera: Braconidae). Micron. 2007; 38:684-693.
18. Onagbola EO, Fadamiro HY. Scanning electron microscopy studies of antennal sensilla of Pteromalus cerealellae (Hymenoptera: Pteromalidae). Micron. 2008; 39: 526-535.
19. Dweck HK. Antennal sensory receptors of Pteromalus puparum female (Hymenoptera: Pteromalidae), a gregarious pupal endoparasitoid of Pieris rapae. Micron. 2009; 40: 769-774.
20. Onagbola EO, Boina DR, Hermann SL, et al. Antennal sensilla of Tamarixia radiata (Hymenoptera: Eulophidae), a parasitoid of Diaphorina citri (Hemiptera: Psyllidae). Ann Entomol Soc Am. 2009; 102: 523-531.
21. Das P, Chen L, Sharma KR, et al. Abundance of antennal chemosensilla in two parasitoid wasps with different degree of host specificity may explain sexual and species differences in their response to host-related volatiles. Microsc Res Tech. 2010; [Epub ahead of print].
22. Wang X, Yang Z, Gould JR, et al. Sensilla on the antennae, legs and ovipositor of Spathius agrili Yang (Hymenoptera: Braconidae), a parasitoid of the emerald ash borer Agrilus planipennis Fairmaire (Coleoptera: Buprestidae). Microsc Res Tech. 2010; 73: 560-571.
23. Norton WN and Vinson SB. Antennal sensilla of three parasitic Hymenoptera. Int J Insect Morphol and Embryol. 1974; 3: 305-316
24. Tegoni M, Campanacci V, Cambillau C. Structural aspects of sexual attraction and chemical communication in insects. Trends Biochem Sci. 2004; 29: 257-264.
25. Pelosi P, Calvello M, Ban L. Diversity of odorant-binding proteins and chemosensory proteins in insects. Chem Senses. 2005; 30(suppl 1): i291-i292.
26. Peng G, Leal WS. Identification and cloning of a pheromone-binding protein from the Oriental beetle, Exomala Orientalis. J Chem Ecol. 2001; 27: 2183-2192.
27. Riviere S, Lartigue A, Quennedey B, et al. A pheromone-binding protein from the cockroach Leucophaea

maderae: cloning, expression and pheromone binding. Biochem J. 2003; 371: 573-579.
28. Vogt RG, Rogers ME, Franco M, et al. A comparative study of odorant binding protein genes: differential expression of the PBP1-GOBP2 gene cluster in Manduca sexta (Lepidoptera) and the organization of OBP genes in Drosophila melanogaster (Diptera). J Exp Biol. 2002; 205: 719-744.
29. Vogt RG, Callahan FE, Rogers ME, et al. Odorant binding rotein diversity and distribution among the insect orders, as indicated by LAP, an OBP-related protein of the true bug Lygus lineolaris (Hemiptera, Heteroptera). Chem Senses. 1999; 24: 481-495.
30. Krieger MJ, Ross KG. Molecular evolutionary analyses of the odorant-binding protein gene Gp-9 in fire ants and other Solenopsis species. Mol Biol Evol. 2005; 22: 2090-2103.
31. Ishida Y, Chiang VP, Haverty MI, et al. Odorant-binding proteins from a primitive termite. J Chemi Ecol. 2002; 28: 1887-1893.
32. Picimbon JF, Gadenne C. Evolution of noctuid pheromone binding proteins: identification of PBP in the black cutworm moth, Agrotis ipsilon. Insect Biochem Mol Biol 2002; 32: 839-846.
33. 33. Ban L, Scaloni A, D'Ambrosio C, et al. Biochemical characterization and bacterial expression of an odorant-binding protein from Locusta migratoria. Cell Mol Life Sci. 2003; 60: 390-400.
34. McKenna MP, Hekmat-Scafe DS, Gaines P, et al. Putative Drosophila pheromone-binding proteins expressed in a subregion of the olfactory system. J Biol Chem. 1994; 269: 16340-16347.
35. Robertson HM, Martos R, Sears CR, et al. Diversity of odourant binding proteins revealed by an expressed sequence tag project on male Manduca sexta moth antennae. Insect Mol Biol. 1999; 8: 501-518.
36. Marchese S, Angeli S, Andolfo A, et al. Soluble proteins from chemosensory organs of Eurycantha calcarata (Insects, Phasmatodea). Insect Biochem Mol Biol. 2000; 30: 1091-1098.
37. Picimbon JF, Dietrich K, Angeli S, et al. Purification and molecular cloning of chemosensory proteins from Bombyx mori. Arch Insect Biochem Physiol. 2000; 44: 120-129.
38. Calvello M, Guerra N, Brandazza A, et al. Soluble proteins of chemical communication in the social wasp Polistes dominulus. Cell Mol Life Sci. 2003; 60: 1933-1943.
39. Wanner K, Willis L, Theilmann DA, et al. Analysis of the insect OS-D-like gene family. J Chem Ecol. 2004; 30: 889-911.
40. Jacobs SP, Liggins AP, Zhou JJ, et al. OS-D-like genes and their expression in aphids (Hemiptera: Aphididae). Insect Mol Biol. 2005; 14: 423-432.
41. Shin DH, Lee JY, Hwang KY, et al. High-resolution crystal structure of the non-specific lipid-transfer protein from maize seedlings. Structure. 1995; 3: 189-199.
42. Sandler BH, Nikonova L, Leal WS, et al. Sexual attraction in the silkworm moth: structure of the phermone-binding-protein-bombykol complex. Chem Biol. 2000; 7: 143-151.
43. Horst R, Damberger F, Luginbühl P, et al. NMR structure reveals intramolecular regulation mechanism for pheromone binding and release. Proc Natl Acad Sci U S A. 2001; 98: 14374-14379.
44. Xu Y, He P, Zhang L, Fang S, et al. Large-scale identification of odorant-binding proteins and chemosensory proteins from expressed sequence tags in insects. BMC Genomics. 2009; 10: 632.
45. Zhou J. Odorant-binding proteins in insects. Vitam Horm. 2010; 83:241-272.
46. Prestwich GD. Bacterial expression and photoaffinity labeling of a pheromone binding protein. Protein Sci. 1993; 2: 420-428.
47. Pelosi P, Maida R. Odorant binding proteins in vertebrates and insects: Similarities and possible common function. Chem Senses. 1990; 15: 205-215.
48. Pophof B. Pheromone-binding proteins contribute to the activation of olfactory receptor neurons in the silkmoths Antheraea polyphemus and Bombyx mori. Chem Senses. 2004; 29: 117-125.
49. Kaupp UB. Olfactory signaling in vertebrates and insects: differences and commonalities. Nat Rev Neurosci. 2010; 11: 188-200.
50. Li L, Miller DR, Sun J. The influence of prior experience on preference and performance of a cryptoparasitoid Scleroderma guani (Hymenoptera: Bethylidae) on beetle hosts. Eco Entomol. 2009; 34: 725-734.
51. Lu D, Li X, Liu X, et al. Identification and Molecular Cloning of Putative Odorant-Binding Proteins and Chemosensory Protein from the Bethylid Wasp, Scleroderma guani Xiao et Wu. J Chem Ecol. 2007; 33:1359-1375.
52. Kyhse-Andersen J. Electroblotting of multiple gels: a simple apparatus without buffer tank for rapid transfer of proteins from polyacrylamide to nitrocellulose. J Biochem Biophys Methods. 1984; 10: 203-209.
53. Hekmat-Scafe DS, Scafe CR, McKinney AJ, et al. Genomewide analysis of the odorant-binding protein gene family in Drosophila melanogaster. Genome Res. 2002; 12: 1357-1369.
54. Schneider, D. Insect antennae. Annu Rev Entomol. 1964; 9:103-122.
55. Altner, H. Insect sensillum specificity and structure: an approach to a new typology. In: Magnen J and MacLeod P, ed. Olfaction and taste VI (Paris). London: Information Retrieval; 1977: 295-303.
56. Pelletier J, Leal WS. Genome analysis and expression patterns of odorant binding proteins from the southern house mosquito Culex pipiens quinquefasciatus. PLoS One. 2009; 4: e6237.
57. Zhou J, Kan Y, Antoniw J, et al. Genome and EST analyses and expression of a gene family with putative functions in insect chemoreception. Chem Senses. 2006; 31: 453-465.
58. Zhou J, He X, Pickett JA, et al. Identification of odorant binding proteins of the yellow fever mosquito Aedes aegypti, genome annotation and comparative analyses. Insect Mol Biol. 2008; 17: 147-163.
59. Zhou J, Robertson G, He X, et al. Characterisation of Bombyx mori odorant-binding proteins reveals that a general odorant-binding protein discriminates between sex pheromone components. J Mol Biol. 2009; 389: 529-545.
60. Lartigue A, Campanacci V, Roussel A, et al. X-ray structure and ligand binding study of a moth chemosensory protein. J Biol Chem. 2002; 277: 32094-32098.
61. Ishida Y, Chiang V, Leal WS. Protein that makes sense in the Argentine ant. Naturwissenschaften, 2002; 89: 505-507.
62. Calvello M, Brandazza A, Navarrini A, et al. Expression of odorant-binding proteins and chemosensory proteins in some Hymenoptera. Insect Biochem Mol Biol. 2005; 35: 297-307.
63. Nagnan-Le Meillour P, Cain AH, Jacquin-Joly E, et al. Chemosensory Proteins from the Proboscis of Mamestra brassicae. Chem Senses. 2000; 25: 541-553.
64. Kitabayashi AN, Arai T, Kubo T, et al. Molecular cloning of cDNA for p10, a novel protein that increases in the regenerating legs of Periplaneta americana (American cockroach). Insect Biochem Mol Biol. 1998; 28: 785-790.
65. Dietz A, Humphreys WJ. Scanning electron microscopic studies of antennal receptors of the worker honey bee, including sensilla campaniformia. Ann Entomol Soc Am. 1971; 64: 919-925.
66. Gramacho KP, Gonçalves LS, Stort AC, et al. Is the number of antennal plate organs (sensilla placodea) greater in hygienic than in non-hygienic Africanized honey bees? Genet Mol Res. 2003; 2: 309-316.
67. Monteforti G, Angeli S, Petacchi R, et al. Ultrastructural characterization of antennal sensilla and immunocytochemical localization of a chemosensory protein in Carausius morosus

Brünner (Phasmida: Phasmatidae). Arthropod Struct Dev. 2002; 30: 195-205.
68. Isidoro N, Romani R, Bin F. Antennal multiparous sensilla: their gustatory features for host recognition in female wasps (Insecta, Hymenoptera: Platygastroidea). Microsc Res Tech. 2001; 55: 350-358.
69. Hekmat-Scafe DS, Steinbrecht RA, Carlson JR. Coexpression of two odorant-binding protein homologs in Drosophila: implications for olfactory coding. J Neurosci. 1997; 17: 1616-1624.
70. Shanbhag SR, Hekmat-Scafe D, Kim MS, et al. Expression mosaic of odorant-binding proteins in Drosophila olfactory organs. Microsc Res Tech. 2001; 55: 297-306.
71. Maida R, Mameli M, Mueller B, et al. The expression pattern of four odorant-binding roteins in male and female silk moths, Bombyx mori. J Neurocytol. 2005; 34: 149-163.
72. Sa´nchez-Gracia A, Vieira FG, Almeida FC, et al. Comparative genomics of the major chemosensory gene families in arthropods. Chichester: Encyclopedia of Life Sciences (ELS), John Wiley & Sons. 2011.